# CHAPTER 6

# PERFORMANCE IMPROVEMENT TECHNIQUES FOR MILO

## 6.1 Introduction

To characterize different propagation parameters, like, shunt capacitance and series inductance per unit length, etc. to control the dispersion characteristics, with and without beam has been discussed in chapter 4 and 5. In this chapter the analysis developed in chapter 4 and 5 have been used to optimize the MILO beam and structure parameters. Beam-wave interaction studies and performance improvement methods for the MILO have been investigated analytically as well as using 3D PIC simulation. The results concluded have been validated with those obtained through RF analysis for HPM device MILO employing equivalent circuit approach. S-Band MILO is presently under development in India in which our research group is also involved. Present work is focused to improve RF output power and efficiency of various variant of MILO structure.

### 6.2 Limitations of Conventional MILO

The key operational parameters for a MILO structure are peak power, efficiency, pulse duration or energy per pulse. Maximizing power and efficiency are active research area taking into consideration various beam and structure parameters. Now-a-days, high power microwave devices such as VIRCATOR, MILO are needed in many HPM system applications. The virtual cathode oscillator, BWO, relativistic magnetron and MILO are promising high power microwave sources and major hotspots in the field of HPM research. The major problem encountered in devices is that their power conversion efficiencies are not very high. In MILO device, limitation is encountered, due to fact that a large fraction of the DC input current forms the load current [Lemke *et al*. (1997)]. Azimuthal self magnetic field is generated due to the load (or critical) current. This magnetic field is needed to guide the initially radial beam into an axial flow and has no contribution in the generation of the RF energy.

Thus, only two-third of load current could be utilized properly. This happens due to fact that during operation, all the load current is not getting utilized because large part of cathode is under the collector [Cousin *et al.* (2005), Lemke *et al.* (1997), Dwivedi and Jain (2013)]. Thus, further investigations are necessary for the performance improvement and necessary to develop a criterion for increasing the power conversion efficiency of the MILO device. This can be achieved if we are able to utilized load current that lead to maximizes feedback. In addition to this, the length of emitting cathode extending downstream of extractor gap (load region) must be set properly to achieve maximum power. By forcing the emitted current under the collector which is equal to the minimum current needed to insulate the electron flow under the periodic resonator, one can optimize the electron flow profile that helps in optimizing quality factor. This improvement is possible only by reducing the length of cathode under the collector or beam dump disk and stubs. This process ensures maximum energy transfer from the beam electrons to the modes of the periodic resonator. In Chapter 3, simulation analysis of improved MILO structure is described; where the only difference between the conventional MILO and Modified MILO is in construction of the load region that comprised of a beam dump disk and the inner conductor of the output coaxial transmission line. This structural change helps in reducing the overall length of device.

### 6.3 Performance improvement through MILO parameters optimization

In chapter 3, design and simulation analysis of improved MILO structure is described. In the present chapter, various steps are defined to improve the performance of improved MILO. This is being done through power and energy expression defined in chapter 5.

### 6.3.1 Optimization through structure and beam parameters

In order to maximize device efficiency, RF coupling between output coaxial transmission line or beam dump disk has also to be optimized. This can be achieved through optimizing the extractor radius, considering internal and external quality factor. For proper transfer of RF power to the external load, extractor radius play an important role.

#### *6.3.1.a Optimization of the extractor in term of quality factor*

Extractor is one of the major subsection of MILO design for extracting power out from the device. In MILO, RF power is extracted axially and for efficient power extraction it is important to couple the oscillation cavity with the output coaxial transmission line. Here, extractor provides such coupling and fixes the opening by which power is extracted and propagated towards outside. The Extractor part includes last MILO vane (called Extractor vane) and the axial distance from the extractor vane and the coaxial transmission line (called the Extractor gap). The inner radius of the extractor vane is slightly larger than the rest of the vanes to provide a good match of the extractor gap electric field to that of the output coaxial transmission line (CTL). In the extractor section, RF standing wave is converted into the travelling wave which has to be propagated outside. MILO device oscillates on the $\pi$ mode and energy is stored in the form of standing wave inside cavity. This standing wave is converted into travelling wave by the extractor. The energy stored inside cavity is coupled with the load through coaxial line with the output opening axially. The interaction cavities coupling with the load may be either over-coupled or under-coupled depending upon the external Q-factor and in both cases electromagnetic energy can be extracted out.

- When $Q_{ext}=Q_{int}$, the energy dissipation in the resonant cavity and that of load are equal. This is called critical coupling.

- When $Q_{ext} < Q_{int}$, the energy dissipation in the resonant cavity is less than that in the load and such coupling is called over-coupling or on-coupling.
- When $Q_{ext} > Q_{int}$, the energy dissipation in the resonant cavity is greater than that in the load and such coupling is called Under-coupling.

For energy to be coupled out efficiently; there should be over-coupling between cavity and load. The radius of extractor cavity affects the external Q-factor and thus the output power coupled with the load. The coupling coefficient of the cavity, α, can be estimated using following relation:

$$\frac{Q_{ext}}{Q_{int}} = \frac{Z_0}{R} = \alpha \quad .$$

If α < 1 the external losses via the waveguide are higher than the internal losses in cavity and Cavity is known as over-coupled. The optimization of the extractor radius for efficient power extraction shows that at extractor vane radius of 54 mm maximum external Q-factor is attained shown in Figure 6.1.

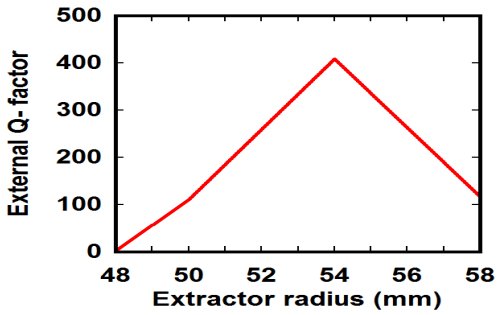


**Figure 6.1:** $Q_{ext}$ variation with $R_{ext}$.

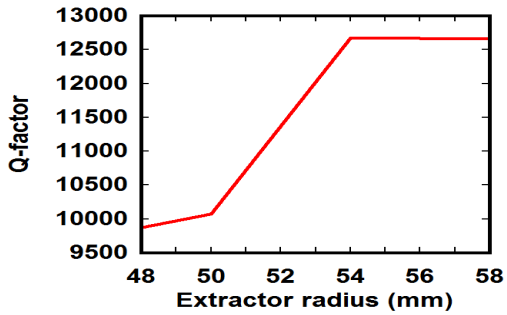


**Figure 6.2:** $Q_{int}$ factor variation with $R_{ext}$.

It has been shown in the Figure 6.2 that the $Q_{int}$ factor is much higher in magnitude and at extractor radius $R_{ext}$ ~ 54 mm it attains its maximum value. It has been revealed by Haworth *et al.* that by optimizing the collector outer radius, in conjunction with extractor vane inner radius, efficiency can be increased. The variation in quality factor with the extractor radius is tabulated in Table 6.1.

**Table 6.1:** Variation of extractor radius with cavity quality factor and coupling coefficient.

| Extractor radius (mm) | External Q-factor | Internal Q-factor | Coupling coefficient of the cavity α |
|---|---|---|---|
| 48 | 2.274 | 9868 | Over-couple |
| 50 | 110.4 | 10077 | Over-couple |
| 54 | 408 | 12673 | Over-couple |
| 58 | 116.5 | 12660 | Over-couple |

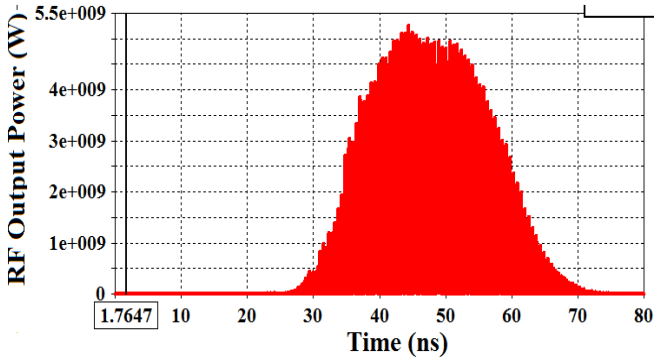


**Figure 6.3:** Temporal RF output power at desired mode.

Thus to improve power conversion efficiency of improved MILO, considering above concept and ref. [Cousin *et al.* (2005)], inner radius of collector should be equal to extractor vane inner radius to provide good match between extractor gap electric field and output coaxial transmission line. This is the first step for improvement. From above figures, it has been concluded that for efficient extraction, radius should be 54 mm, and corresponding quality factor can be determined from Figures 6.1 and 6.2. Secondly, optimizing the distance between extractor vane radius and stubs helps in improving efficiency. Distance should be equal to $\lambda_g/4$ to achieve maximum and stable RF output power. Instead of two stubs, here four stubs are used that helps in proper magnetic insulation and maximizes feedback. During simulation, maximum RF output power that is achieved is 5 GW at a peak resonant frequency of 1.76 GHz. Considering same structure and beam parameters as mentioned in Chapter 3, improved RF output power generated is shown

in Figure 6.3. Instead of two stubs, here four stubs are used that helps in proper magnetic insulation and maximizes feedback. During simulation, maximum RF output power that is achieved is 5 GW at a peak resonant frequency of 1.76 GHz.

Considering the power expression for RF output power in Chapter 5, the temporal RF output power implementing above improvement is validated against simulation. Considering expressions (5.47) and (5.51) and other relevant expressions defined in previous chapter, improved MILO RF output power, energy released and temporal growth rate is shown in Figure 6.4 for typically design parameters defined in Chapter 3.

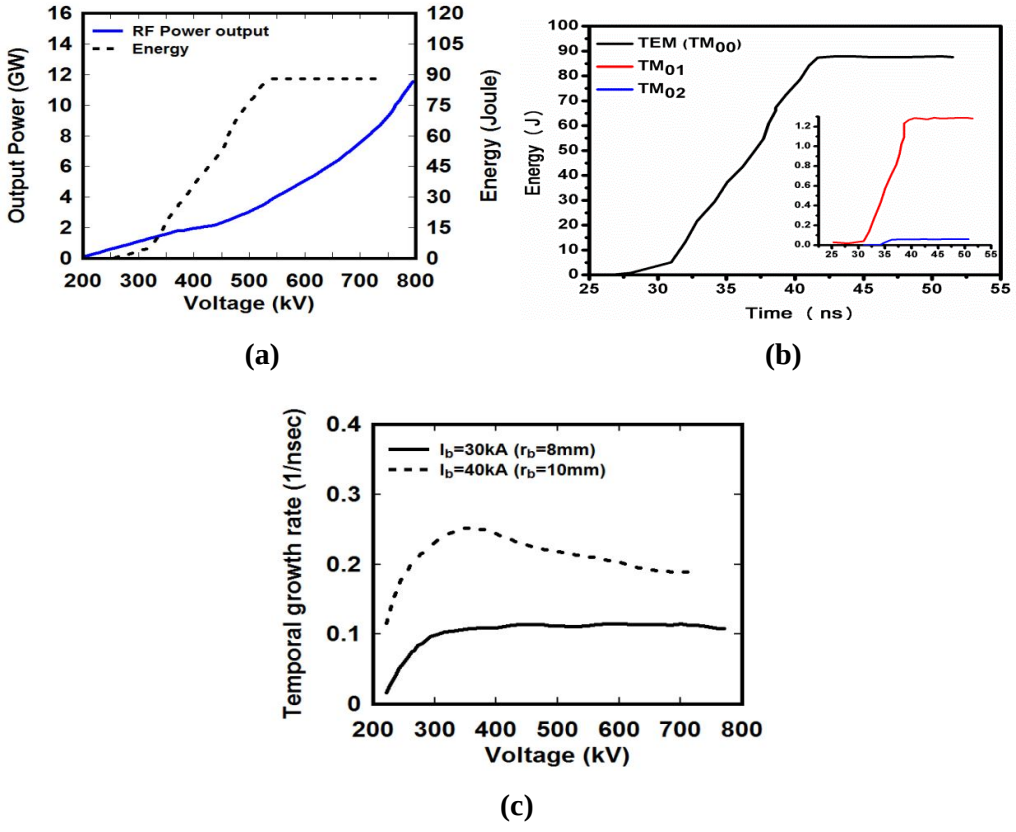


**Figure 6.4:** **(a)** Variation of RF output power with voltage using analysis, **(b)** RF energy developed during simulation, **(c)** Variation of growth rate with voltage.

For different beam voltage the RF power generated has been calculated considering Figure 6.4(a). During numerical analysis structure parameters mentioned in chapter 3 are used for expression for RF power derived in chapter 5. It has been concluded from the same plot that maximum energy released is 90J for improved MILO structure in chapter 3. It has been concluded from Figure 6.4(b) that fundamental mode stores maximum energy and the amount of energy transfer to other competiting modes. Figure 6.4 (c) is the plot of normalized growth rate versus applied voltage for magnetically insulated flow for different beam radii using equation (5.36).

### *6.3.1.b. Optimization of the Cathode Radius*

HPM source design can be improved by employing analytical modeling using different techniques, as given in Chapters 4 and 5. Further, improvement is done using PIC simulation to provide guidance to validate the design of source. This is perhaps a first step toward an optimum HPM source. It has been reported that for designing HPM tubes for long pulses, field strengths in the cavities and SWS should be kept below 150 kV/cm. This step will help avoid unintended plasma generation. In order to avoid pulse shortening, cathode area study is the point of innovation. Beam current develop inside the structure depend on the cathode radius and anode radius as can be seen from different expressions given in Chapter 2. Variation of anode or beam current with radius of cathode is shown in Figure 6.5.

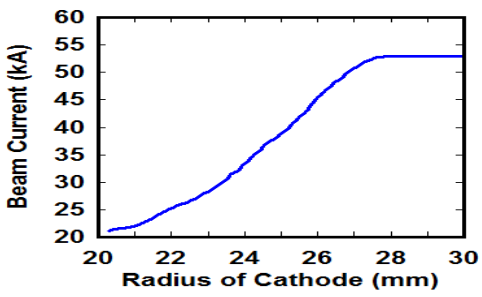


Figure 6.5: Variation of beam current with radius of cathode.

### *6.3.1.c. Optimization of load parameters*

This optimization is being taking into account here, to validate the idea reported by Lemke *et al.* (1997). It has been reported by Lemke that power is inversely proportional to load length. The load region of MILO comprises of the part of cathode inside collector (load length) and the collector cavity depth. Electron current flow through load side generates the required azimuthal magnetic field which insulates the electron flow in the SWS region. Critical current required for magnetic insulation can be calculated using the known expression,

$$I_{cr} = I_{\alpha} g \gamma_a \beta_a \quad .$$

Here $I_{\alpha} = 8.5$ kA, $\beta_a$ is the electron drift velocity divided by the speed of light ($c$) evaluated at anode, $\gamma_a = 1/\sqrt{1-\beta_a^2}$, and $g = 377/(2\pi Z_0)$ with $Z_0 = \ln(r_a / r_c)$, $r_a$ anode radius and $r_c$ cathode radius. In load-limited MILO [Lemke *et al.* (1997)], emission surface of the cathode was along the curved part of the cylindrical cathode. Required critical current for magnetic insulation provided by this load length, calculated by Lemke *et al.* (1997) following relations:

$$L_{\min} = 2 r_c \ln\left(\frac{r_a}{r_c}\right) \frac{(\gamma_a^2 - 1)^{1/2}}{F(\gamma_a)^2}$$

Where $F(\gamma_a) = \int_1^{\gamma_a} \frac{1}{(\gamma^2 - 1)^{1/4}} d\gamma$ , $\gamma$ is the relativistic factor due to applied beam voltage and $\gamma_a$ is the relativistic factor close to the anode end. Improvement in load length is done by Fan *et al.* (2007) in which the emission surface of cathode comprised of both the right end and the end surfaces of the cathode. With this improvement, the required load length for magnetic insulation has been deceased. Half of the load current required for magnetic insulation in the SWS region provided by the end surface of the cathode. It has been observed that load length affect the output power of the device and hence the overall performance. Collector is used to collect the electrons after

beam-wave interaction but, more of the collected electrons do not take part in further beam-wave interaction. Figure 6.6 shows the effect of load length variation on output power keeping fix collector cavity depth. This load length forms feedback path and the collector cavity depth works as the capacitor. This capacitor helps to extract out RF energy from the collector as well as from SWS cavities. The capacitance here decreases with increase in collector cavity depth and decrease in load length. Maximum output power obtain at load length of 5mm to 10 mm.

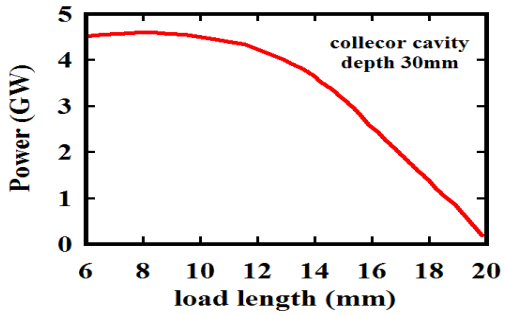


**Figure 6.6:** Variation of output power Vs load length at fixed collector depth ~30 mm.

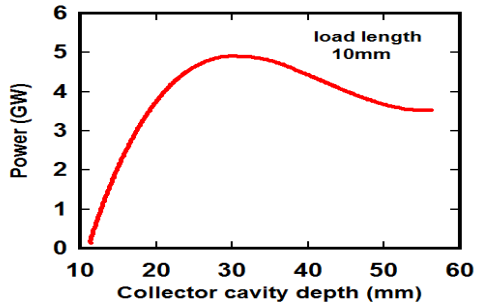


**Figure 6.7:** Variation of output power Vs collector cavity depth at fixed load length ~10mm.

Figure 6.7 shows the variation of output power with collector cavity depth for 10 mm fixed load length. It can be seen from figure that output power initially increases with increase in collector cavity depth upto 30 mm and then decreases. Optimization of the load parameters shows that maximum beam-wave interaction takes with the collector cavity of 25 to 30 mm and corresponding load length of 5 mm to 10mm. With this optimized parameter high-power microwave is generated with

peak power of 5 GW, frequency of 1.76 GHz, and power conversion efficiency about 16%. The effect of load parameters on a typical L-band MILO reported in literature has been studied in detail using commercial PIC simulation code 'CST Particle Studio'. The study of load parameters effect has been carried out with different load length and collector cavity depth. At optimum load length of 10mm and collector cavity depth of 30mm, output peak power of 5 GW generated at 1.76 GHz frequency. The enhancement in RF output power and efficiency has been observed around 16% in comparison to results reported by Fan *et al.* (2007).

#### *6.3.1.d. Need of Optimizing load length*

For proper beam-wave interaction process in MILO, $L_{col} \geq L_{c,min}$ so that the electric circuit is closed by the load under the collector. The recovery length of collector on cathode makes it possible to lengthen the duration of microwave pulse. Length of cathode inside the collector (load length) produces critical current $I_{cr}$ and is important for magnetic insulation inside the device. When the load length ($L_{c,min}$) is longer than the minimum length required generating critical current, it behaves like an MITL. Microwaves that get into this region are partially absorbed by the insulated portion of the flow, which reduces feedback. Therefore, emitting cathode length should be kept beyond the extractor gap, so that it is the minimum necessary to produce the cutoff current in the load ensure maximizes feedback. An expression for the minimum load length is obtained by setting the product of child–Langmuir current density and the cathode surface area equal to critical current. Load length is also responsible for energy extraction and forms an additional cavity. The additional cavity which is at the load side works as capacitor. This capacitor is used to store less energy inside the collector but make effective coupling with the energy storing SWS part. As $C = \frac{\varepsilon_0 A}{d}$

here *d* is the axial depth of collector cavity. As value of *d* increases then *C* decreases. It forms feedback path structure up to the length of the cathode under collector and remaining part of the collector forms additional cavity. Thus, by forcing the emitted current under the collector to be equal to the minimum current needed to insulate the electron flow under the SWS resonator, optimization of Load length required. Minimum length required to produce critical current is calculated using relation:

$$L_{c,\min} = 1.6 \frac{d^2}{r_c \ln(r_a / r_c)} \left( \frac{\sqrt{\gamma_0 + 1}}{\gamma_0 - 1} \right) \quad .$$

In above equation, anode radius, $r_a$, should be kept equal to the SWS cavity inner radius, *d* is the difference between inner radius of collector and radius of cathode.

### *6.3.1.e Effect of distance between extractor cavity and the stub*

Studies indicate that the distance between the stubs and the last vane or extractor cavity can affect the operation characteristics of the device. The load (the inner conductor) and the waveguide form the coaxial line which permits the extracted microwave to transmit outside. The distance between the extractor cavity and the stub can be calculated while considering distance $\lambda_g/4$, where $\lambda_g$ is the waveguide wavelength. Stub provides short circuit at distance $\lambda_g/4$ which works as open circuit stub. The main advantage of stubs is to radiate TM wave with minimum losses due to reflection through stub. The waveguide radius ($\lambda_g$ ) can be estimated using relation:

$$\lambda_g = \lambda / \sqrt{1 - (f_c / f)^2} \, ,$$

where $f_c$ and *f* are the cut-off and operating frequency, respectively. If the radius of extractor cavity is larger than the rest of the cavities the impedance matching to output coaxial line, that transmits the radiated RF energy to the output antenna, would be better. Hence to extract RF energy, it is necessary to couple the oscillator cavity with the output waveguide. Stubs are made of the conducting rods which grounded the

inner conductor of output coaxial transmission line to the anode and having low impedance. It has to be noticed that the load current provides self magnetic field that helps to insulate the flow in the SWS region. The inductance of the rods is large enough so that they do not perturb the radiated microwaves. Stub is inductive in nature having impedance $|z_L| = \omega L$, for DC $\omega = 0$ and for RF $\omega$ is very high so it works as DC short and RF open. The inductance of the rods is large enough to perturb the axial radiation of the microwaves. Stub also provides support to the output coaxial transmission line. Implementation of stubs provides pure frequency spectrum and the RF output power is more stable.

## 6.4 Efficiency Enhanced L-band MILO

Previously described sub-sections validate the simulation analysis while considering analytical approach mentioned in Chapter 5. Figure 6.8, represents schematic of efficiency enhanced L-band MILO. Optimizing the distance between extractor cavity and stubs; and optimizing various load parameters led to increase in power conversion efficiency from 12 to 16%. It is well known that the operation of MILO needs well insulating magnetic field. Improper insulating field reduces the energy of the electron beam coupling into the RF electromagnetic wave. Henceforth, it becomes difficult to adjust the insulating magnetic field in the conventional MILO because no part of it can be moved easily. Now, another step for increasing efficiency is to insert foil or conducting disk inside the beam dump that helps in improving efficiency.

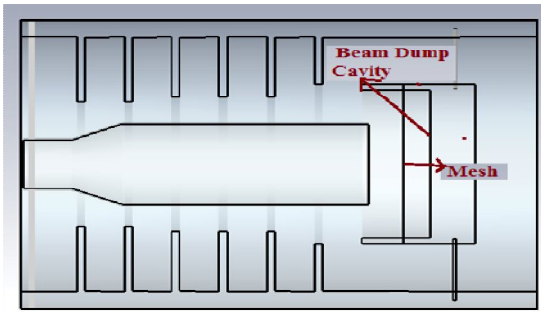


**Figure 6.8:** Schematic of efficiency enhanced L-band MILO.

In order to control the insulating magnetic field, a new beam dump with reflector has been employed which rendered several advantages:

- The distance between the end surface of cathode and the reflector affect the load current and hence the DC magnetic field between the tip of discs and cathode. Due to reflection of electrons, from the foil, current modulation takes place which further led to density modulation of electrons hence improved beam-wave interaction takes place.
- In the improved MILO with reflector inside the beam dump, electrons of load current is provided by the reflector instead of the end surface of cathode extended into the beam dump region.
- In conventional MILO, beam electrons that get into inserted part of cathode are partially absorbed by the insulated portion of the flow which reduces feedback and also do not take part during RF generation. Therefore by fixing the length of the emitting cathode beyond the extractor gap, it is the minimum necessary step to produce the cutoff current in the load. This ensures maximum feedback of load current towards the slow wave structure.

### 6.4.1 Simulation Results

When a conducting foil introduced inside the beam dump, it increases RF output power due to the involvement of maximum feedback mechanisms. It is only possible when inner radius of beam dump is equal to the extractor inner radius. It creates proper resonance between extractor gap and interaction structure. Thus, maximum coupling of RF takes place between extractor gap and coaxial transmission line. After optimization, improved MILO structure with reflector or foil resulting RF output peak power ~7 GW and resonate at 1.76 GHz frequency (see Figure 6.9).

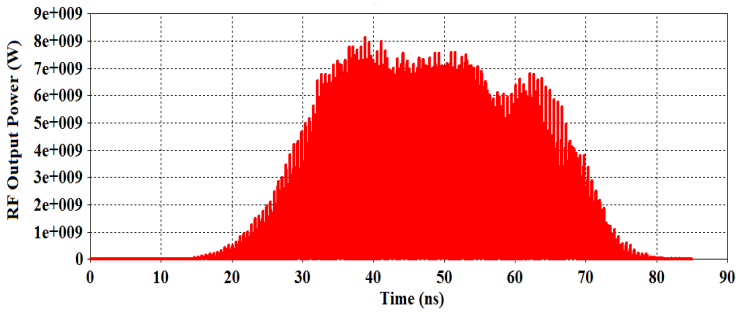


**Figure 6.9:** Temporal RF output power developed at $TM_{01}$ mode in improved MILO.

Trajectories of the particles may also be monitored in 2D or 3D planes which yields perturbation information of the particles in terms of energy, phase and momentum.

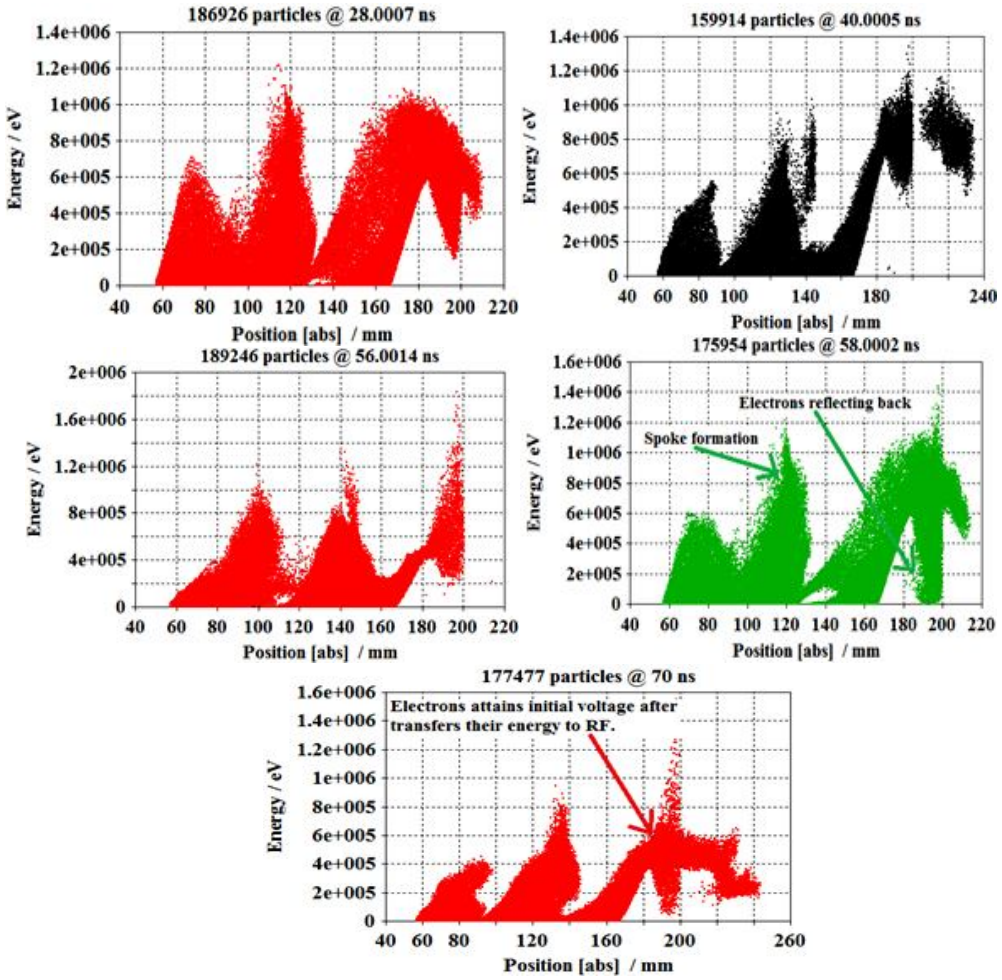


**Figure 6.10:** Energy exchange mechanism during beam-wave interaction process along interaction length of the improved MILO structure.

Using phase-space monitor commands in software, the particles are monitored at a set interval of time over the full or partial time of simulation for their momentum, position etc. Using phase space monitor command, electrons are monitored along the position to acquire the modulation of energy or momentum among particles as shown in Figure 6.10. It has been revealed from Figure 6.10 that as the input voltage increases, axial electric field along the insulated sheath also increases which results in the generation of the space charge waves. These waves induce RF oscillation inside the cavities due to the Diocotron instability. It can be seen from Figures 6.10 that either the alternate spokes are formed or beam-wave interaction takes place when phase velocity of fundamental mode is in synchronism with the drift velocity of beam

electrons. On inserting the foil or mesh into the beam dump significant interaction allow RF energy recovery from the load current. Reflection of electrons from foil position to SWS position, as shown in Figure 6.10 (c-d), leads to an increasing phase velocity. However, the phase focusing and the bunching mechanisms in crossed-field flow, keep electrons synchronize with the wave to allow additional amplification of the RF signal.

## 6.5 Efficiency Enhanced S-band MILO

It has been suggested by various researchers that by adding the end emission from the cathode (for producing axial current) enhances insulated magnetic field. Thus, the requirement of load current may be reduced and the Hull cut-off criterion is satisfied. In this chapter we have presented the improvement in the power conversion efficiency of conventional S-Band MILO considering the principle explained by Dwivedi and Jain (2013) in conjunction with idea given in reference [Fan *et al.* (2007)]. Present scope for the further research is to develop improved S-Band MILO shown in Figure below for increasing the power conversion efficiency. This can only be achieved properly if load current is utilized properly which leads to enhance feedback.

Efficiency of conventional MILO is not much improved due to the uninsulated flow in the beam dump has plasma frequency which is higher than the oscillation frequency [Lemke *et al.* (1997)]. It is anticipated that the application of mesh or foil in inside the beam dump may help to enhance the power conversion efficiency, due to which plasma frequency becomes equal to oscillation frequency. Thus resonant frequency gets matches across the extractor gap and an interaction cavity that results in maximizes power transfer. This study is carried out by considering the properties of

virtual cathode formation as explained in refs. [Champeaux *et al.* (2016), Benford *et al.* (1987)]. We have followed the previously in Chapter 3, design procedure to design S-band tapered cathode MILO which operates at 2.72 GHz, employing DC beam voltage 500 kV and beam current 42 kA. Conventional S-band MILO produces power conversion efficiency ~6% [Dwivedi and Jain (2013)]. Improved design of S-band MILO along with conducting foil or thin disk inside novel beam-dump produces power conversion efficiency ~16.6%. This can be achieved by the configuring a virtual cathode after the foil. This design will facilitate modulation of electron's energy due to improved electrons reflection towards the interaction cavity. The concept of the virtual cathode in magnetically insulated transmission line explained in ref. [Pashchenko]. The improved electron feed backing process led to conversion of density modulation to current modulation which further takes part in beam-wave interaction process. For proper match of extractor gap electric field to that of output coaxial transmission line (CTL), the distance between CTL and the last extractor vane should be kept equal to periodicity between discs. Commercial PIC simulation code MAGIC was used earlier to study the RF behavior of MILO devices [Dwivedi *et al.* (2013), Cousin *et al*. (2005)]. In the present work, a commercial PIC simulation code CST particle studio is used.

### 6.5.1 Optimization of structure parameters

It was anticipated that the modified design of the output coaxial waveguide or beam dump may improve the efficiency. This study is carried out considering the properties of virtual cathode formation as explained in refs [Champeaux *et al.* (2016), Benford *et al.* (1987)]. An S-Band tapered cathode MILO was designed which operates at resonant frequency 2.72 GHz, employing DC beam voltage 500 kV and

beam current 42 kA. Axial depth ($d$, in cm) between cathode and collector cavity is determined using relation [Benford *et al.* (1987)]: $f = \frac{4.77}{d}\ln(\gamma_0 + \sqrt{\gamma_0^2 - 1})$ GHz .

This axial depth ($d$) is responsible for virtual cathode formation inside the beam dump [Benford *et al.* (1985)]. Considering the design equations explained in Chapter 3, various structure and beam parameters can be determined. The improved MILO design specifications are mentioned in Table 6.2.

**Table 6.2**. Design specifications for improved MILO structure.

| **Structure and Beam parameters** | **Specification** |
|---|---|
| Voltage | 500 kV |
| Current | 42 kA |
| Cathode Radius ($r_c$) | 25 mm |
| Anode Radius ($r_a$) | 68 mm |
| SWS Inner Vane Radius | 46 mm |
| Extractor Vane Radius | 49 mm |
| Choke Vane Radius | 41 mm |
| Vane Thickness (T) | 04 mm |
| Periodicity (L) | 17 mm |
| Inner Radius of Beam Dump | 46 mm |
| Length of cathode under collector | 05 mm |

It has been revealed by simulation that to achieve the maximum and stable RF output power, the distance between extractor cavity and stub should be $\lambda_g/4$. Here, four stubs are used which helps to maintain proper magnetic insulation and maximizes feedback. Improvement in load length is reported by Fan *et al.* in which the emission surface of cathode comprised of the right end and the end surfaces of the cathode. With this modification the required load length for magnetic insulation has been decreased. Half of the load current required for magnetic insulation in SWS region is provided by the end surface of cathode. It has been observed that the load length affect the output power of the device and hence the overall performance.

Cconsidering the design parameters mention in Table 6.2, structure is modeled using CST-Particle code, as shown in Figure 6.11.

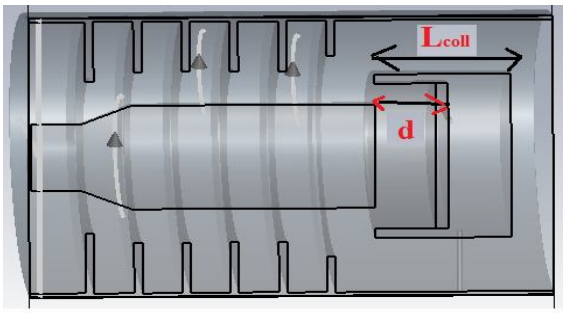


**Figure 6.11:** Schematic of S-band tapered cathode MILO structure.

### 6.5.2 Simulation results

Lemke *et al.* (1997) reported that the load length is inversely proportional to RF output power. Hence by shortening the load length output power should improve. In case of improved MILO the load length of the cathode, inside the beam dump is 05 mm while in conventional MILO the load length is 91 mm. In the improved MILO configuration, it is possible to strengthen the feedback mechanism of the EM wave. Feedback in the cavity increase the amplitude of the energy modulation, since the injected beam current is larger than the space charge limited current of the waveguide [Benford *et al.* (1987)]. Under this condition a part of injected electrons are being reflected back due to the formation of virtual cathode after the conducting disk. The current modulation of the reflected electron beam results microwave emission. This current modulation is due to the energy modulation of the injected beam which is caused by the electromagnetic wave. As the consequence of current modulation, the RF wave gets magnetic insulated much earlier in comparison to the conventional MILO. In improved MILO structure, conducting disk plays the role of reflector or electron collector which can be verified from the simulation result. During PIC simulation, DC pulse voltage is injected from left boundary using discrete port shown

in Figure 6.11. In order to observe RF output power at $TM_{01}$ mode, the waveguide port is implemented at output circular transmission line. The load section and waveguide forms coaxial transmission line which helps in transmitting developed RF energy to outside. To observe the variation in RF output power at $TM_{01}$ mode which corresponds to the oscillating mode of MILO RF power variation is shown in Figure 6.12.

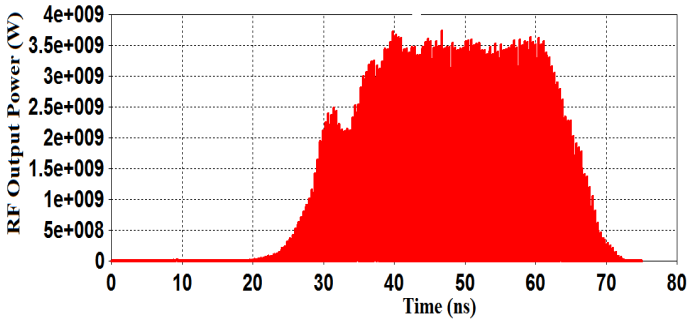


**Figure 6.12:** Temporal RF output power versus time.

In order to validate the resonant frequency of the improved MILO structure, the corresponding oscillation frequency is shown in Figure 6.13. A resonant peak can be seen which affirms the operating frequency of structure.

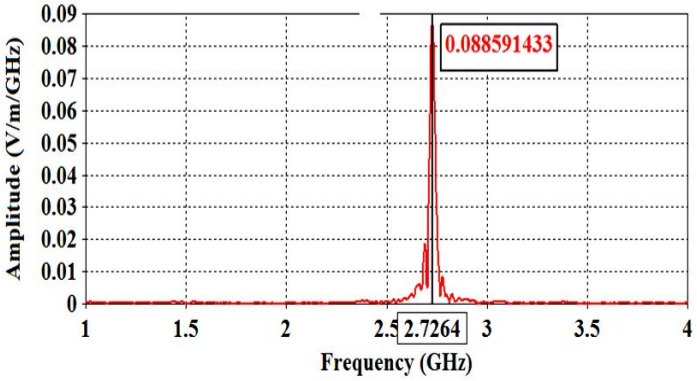


**Figure 6.13:** Frequency spectrum at $TM_{01}$ mode in improved MILO.

MILO operates on the principle of magnetic insulation. During magnetic insulation an insulated electron sheath is formed between tip of discs and cathode as shown in Fig. 6.14. When charging current becomes equal to critical current, magnetic insulation takes place. It can be seen from Fig. 6.14(b) that when electrons

energy become comparable to applied DC voltage, electrons insulate itself between tip of discs and cathode. Electrons present on the insulated sheath consist of both axial electric field and azimuthal magnetic field. Space charge waves are generated due to the repulsion of electrons, acceleration & deceleration of axial electric field. These waves oscillate at plasma frequency which produces noise inside the cavities. Thus, interaction cavities starts oscillating at its natural or resonating frequency, due to which RF voltage induces as shown in Figure 6.14. Initially during magnetic insulation process, some of the electrons get accumulated inside the beam dump that lead to high current density due to space charge effect. At sufficiently high current densities between end surface of cathode and collector, electrons felt the repulsion of other electrons in their neighborhood. So beyond a critical current some of the beam electrons stop and turn back toward the interaction cavities.

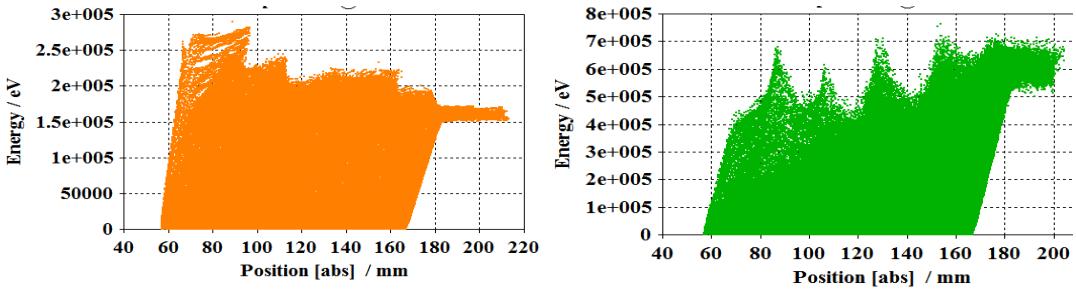


**(a)** **(b)**

**Figure 6.14:** **(a)** Magnetic insulation process at 6ns, **(b)** at 12ns.

This critical current is a characteristic of a drift space and the region in space where electrons slowed down and turn back is known as the virtual cathode. In MILO, RF energy is stored inside the interaction cavities in the form of spokes as shown in Figures 6.15 and 6.17. Beam-wave interaction starts when RF voltage ($V_{RF}$) is greater than the applied DC voltage as shown in Figure 6.15(c). During this interaction spokes are formed inside the cavities when synchronism condition occurs. This condition takes place when drift velocity of electrons becomes equal to phase velocity

of RF wave. This mechanism helps in maintaining external quality factor across the extractor gap equal to internal quality factor across the SWS cavities [Cousin *et al*. (2005)]. Thus maximum RF energy is stored inside the interaction cavity shown in Figure 6.16. It is inferred from Figure 6.15(b) that the electrons are reflected back due to presence of foil at position 200 mm. These electrons are responsible for the formation of virtual cathode. This can be observed by considering momentum phase space monitor plot shown in Figure 6.18.

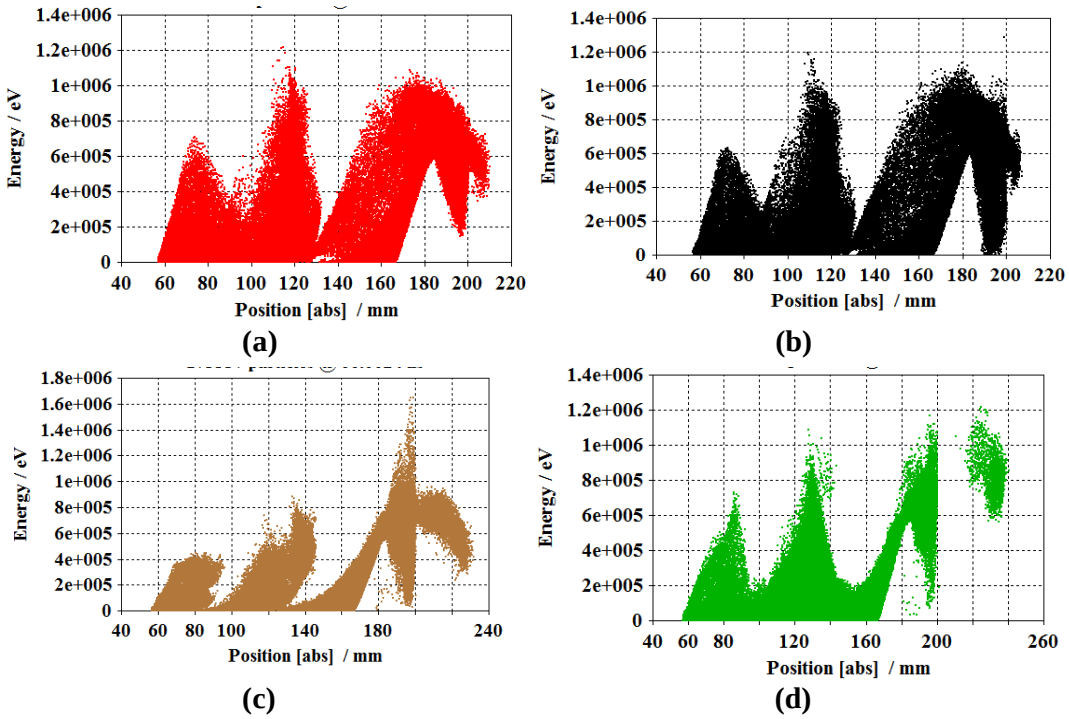


**Figure 6.15:** Distribution of electrons energy along the interaction length.

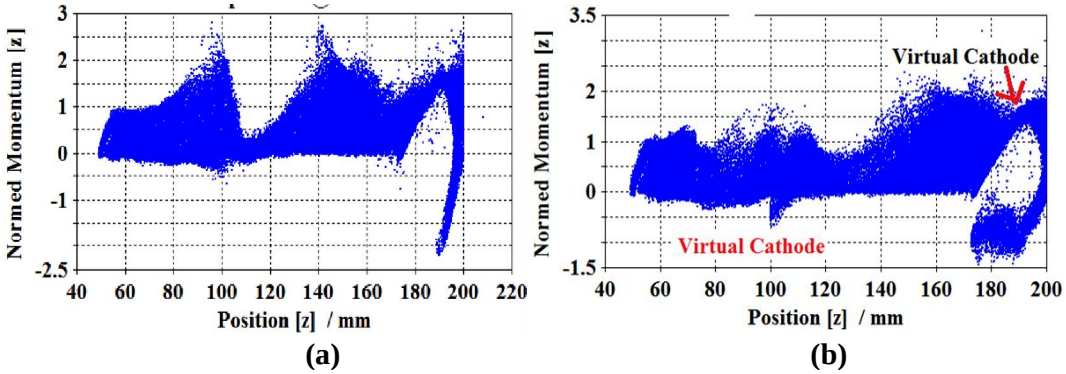


**Figure 6.16:** (a) Electrons reflect back due to foil; and (b) virtual cathode formation.

Foil act as reflector that help in enhancing further beam-wave interaction process. This is achieved due to formation of virtual cathode inside the additional

cavity inside the beam dump. This is formed because beam current exceeds the space charge limiting current [Benford *et al.* (1987)]. Electrons accumulated inside the beam dump reflect back to interaction cavity, which helps in maximizing feedback shown in Figure 6.16(b).

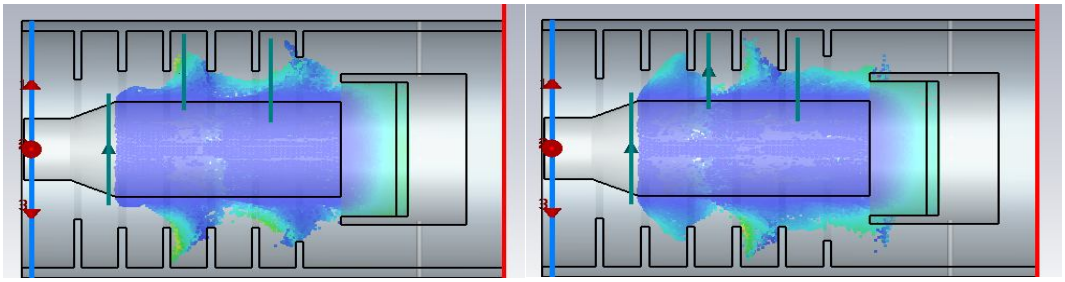

**(a)** **(b)**

**Figure 6.17:** Mechanism of spoke formation during beam-wave interaction.

### 6.5.3 Significance of using conducting disk or foil inside beam dump

In brief, on applying a high DC voltage between anode and cathode, a part of electrons drawn from the cathode surface moves radially while a part of electrons travels towards the beam dump that takes part in the process of magnetic insulation. Beam of electrons accumulated between beam dump disk and inserted cathode part gets density modulated due to the reflection or feedback of electrons from the metal grid with respect to cathode towards the slow wave structure. This process persists because virtual cathode acts as *LC* oscillator [Sullivan (1983), Benford *et al.* (1985)]. Virtual cathode formed beyond the foil behaves as a capacitor to store the beam kinetic energy. When potential across virtual cathode is greater than injected beam energy inside beam dump, bunch of charge is reflected towards the interaction cavities. The electron motion represents a large time varying current through an inductor [Sullivan (1983)]. These density modulated electrons takes part in the generation of RF energy. At this point plasma frequency becomes equal to oscillation

frequency, because uninsulated flow in the beam dump has plasma frequency that is higher than oscillation frequency [Lemke *et al.* (1997)]. Modulation process is achieved due to high electric field region between cathode surface and grid. Due to density modulation, an AC current $J_c$ is established on the electron beam directly at cathode surface. This current is converted to RF energy, through $J_c$. $E_c$ interaction with the circuit electric field $E_c$ inside the SWS. RF energy from the SWS is coupled into output coaxial transmission line, modulating the electron beam at the grid with respect to the cathode. Due to the shorting of space charge field by the transparent grid, space charge limiting current is generated. In presence of this current, cavity develops a potential barrier which stops the passage of electrons, so that electrons are reflected back towards the extractor gap. This feedback mechanism contributes in the generation of RF power [Pashchenko]. Thus, due to the formation of virtual cathode, plasma frequency of electrons across the uninsulated flow is equal to resonant frequency. Manifesting such improvement inside the beam dump helps in increasing the power conversion efficiency of conventional S-Band MILO. Maximum efficiency is accomplished by considering the spokes shown in Figure 6.17, collectively as a modulated dc current crossing a voltage-modulated gap. It has been reveal from Figure, a spoke is on for a half-cycle of the oscillation and is off for the remainder of the cycle, validating pi mode operation. In future authors anticipate validating this theory analytically.

## 6.6 Constant radius cathode S-band MILO

Considering design procedure described in Chapter 3 and also reported by Dwivedi and Jain (2013), in this chapter design specification of an S-band MILO operating at 3 GHz is presented, considering beam voltage ~500 kV and beam current ~47 KA with pulse duration 140ns and rise time 2ns.

**Table 6.3:** Design specifications of S-Band MILO structure.

| Particulars | Radius |
|---|---|
| Choke Cavity Radius | 34 mm |
| Interaction Cavity | 39 mm |
| Extraction Cavity | 49 mm |
| Cathode Radius | 25 mm |
| Disc Periodicity | 13 mm |
| Thickness | 04 mm |
| Load Inner Radius | 44 mm |

Taking into account the above design parameters, a schematic of conventional S-band MILO shown in Figure 6.18.

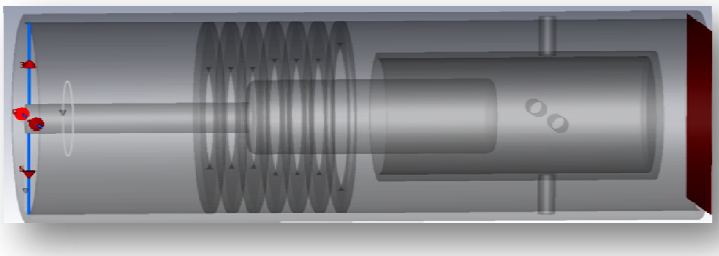

**Figure 6.18:** Schematic of conventional MILO structure.

EM simulation of the RF interaction cavities has been carried to observe the desired operating mode and resonant frequency in the absence of the beam using eigenmode analysis. Using this technique, the presence of a particular mode inside the cavities is confirmed by observing the magnetic field pattern. Figure 6.19 shows the vector plot of electric field of the RF interaction cavities of the MILO which indicates that the desired $TM_{01}$ mode is present inside the cavity. The beam present analysis of MILO is demonstrated by implementing the beam voltage of 500 kV using discrete port at the left end of the interaction structure. During simulation start oscillation current is 17 kA. During simulation process once the pulse voltage is injected from the left side using discrete port that acts as a voltage source available in CST Particle

studio, it is possible to describe the temporal evolution of the electron beam in all the structure. Discrete port is realized as a voltage source.

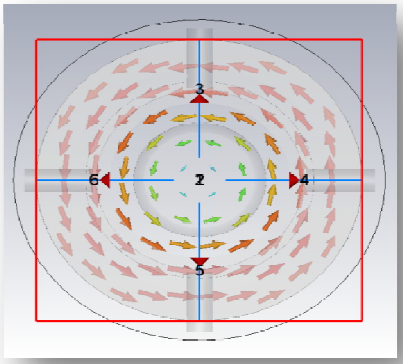


**Figure 6.19:** Developed $TM_{01}$ mode at output port.

In order to observe RF output power at $TM_{01}$ mode, waveguide port is kept at output of circular waveguide as shown in Figure 6.18. Temporal RF output power develop is shown in Figure 6.20.

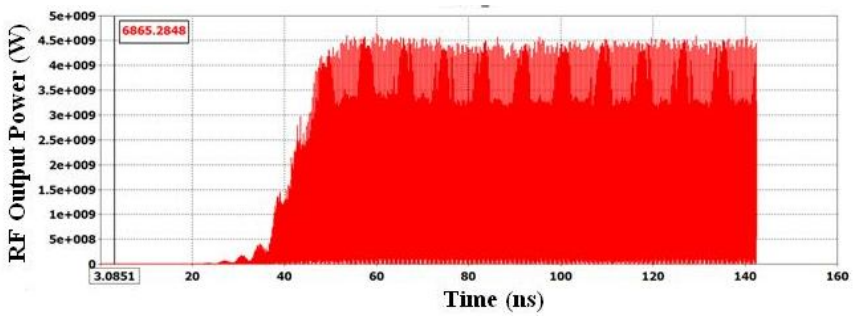


**Figure 6.20:** Temporal growth of RF output power developed at desired mode.

**Expression for Efficiency:** During simulation anode current is 47kA and critical current is 15kA, applied voltage = 500kV thus conversion efficiency is,

$$\eta_{\max} = \frac{P_{\max}}{V_0 I_a} = 0.32\left(1 - \frac{I_{cr}}{I_a}\right)$$

Substituting values in above equation we get conversion/ electronic efficiency 21.7% and the overall efficiency for $P_{in}$=23.5GW and $P_{out}$=3.4GW, then 14.4%. Extraction efficiency= 66.35%; Overall efficiency= electronic*extraction efficiencies.

To improve power conversion efficiency of above structure, optimization is done considering design expressions. This optimization process results in improving total efficiency and reduces overall length of the structure. Inner radius of collector should be equal to radius of interaction cavity and putting $r_a$ = 70mm in expression reported in Chapter 3 also given by Dwivedi and Jain (2013), calculated length of collector = 75.5 mm.

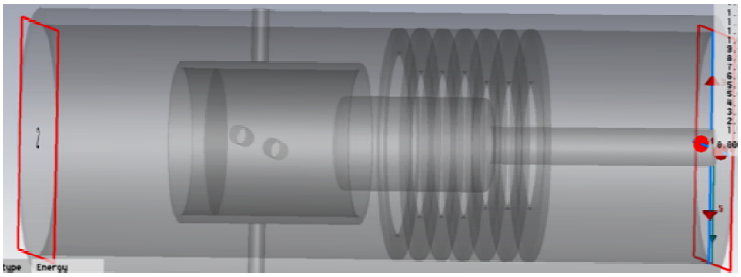

**Figure 6.21:** Schematic of disk-type MILO structure.

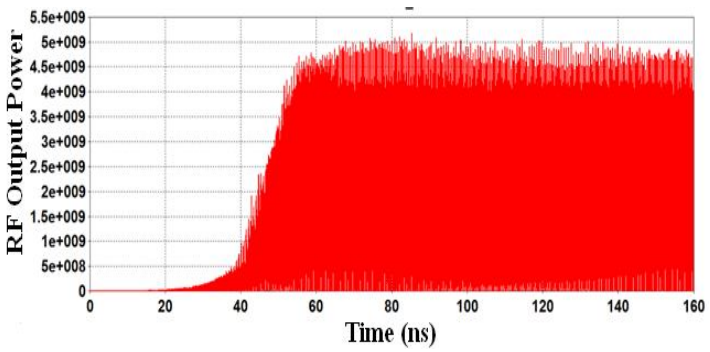


**Figure 6.22:** Temporal RF output power at $TM_{01}$ mode.

**Expression for Efficiency:** During simulation anode current is 50kA and critical current is 12kA, applied voltage = 500kV thus conversion efficiency is,

$$\eta_{\max} = \frac{P_{\max}}{V_0 I_a} = 0.32\left(1 - \frac{I_{cr}}{I_a}\right)$$

Substituting values in above equation we get conversion/ electronic efficiency 24.32% and the overall efficiency for $P_{in}$=25GW and $P_{out}$=4.8GW, then 19.2%. Extraction efficiency= 78.94%; Overall efficiency= electronic*extraction efficiencies.

From above design, it can be concluded that after optimization, power conversion efficiency gets increased.

## 6.7 Conclusion

In this chapter the performance and improvement in MILO structure during beam-wave interaction mechanisms has been carried out. Taking advantage of a reported experimental and simulation work, the beam-wave interaction mechanism of an improved L- and S- band MILO structure operating at desired mode has been described using the CST-PIC simulation software. During simulation employing phase space monitor helps in monitoring at different time instants energy transfer phenomena to RF and mechanisms of spoke formation along interaction length of the electromagnetic structure. Considering salient specifications available in PIC simulation code properly beam-wave interaction mechanisms have been explained including process of magnetic insulation, Brillouin flow and spoke formation of proposed MILO. This is being done here through optimizing various structure and load parameters. Considering various literature reviews reported, a new design is also presented, employing foil inside the beam dump. This process helps in improving power conversion efficiency of MILO structure. For performance improvement, authors optimized simulated L-Band MILO presented in chapter 3. Using design expressions after optimizing various load parameters improved efficiency ~16 %. Inserting grid or reflector inside beam dump results in increased efficiency ~22.4 %. On introducing grid or foil inside the beam dump, results in increasing RF output power due to maximum feedback mechanisms. Conventional S-Band MILO efficiency ~6% , after optimization load parameters and using tapered cathode, power conversion efficiency ~ 16.6%.